Hindawi Publishing Corporation
Journal of Chemistry
Volume 2016, Article ID 8160169, 8 pages
http://dx.doi.org/10.1155/2016/8160169

Research Article

The Influence of Oxygen Substitution on the Optoelectronic Properties of ZnTe

Imad Khan,[1] Sajid Khan,[1,2] Javid Iqbal,[3] H. A. Rahnamaye Aliabad,[4] Zahid Ali,[1] and Iftikhar Ahmad[1]

[1]*Center for Computational Materials Science, Department of Physics, University of Malakand, Chakdara 23020, Pakistan*
[2]*Government Postgraduate College Charsadda, Charsadda 24420, Pakistan*
[3]*Department of Physics, Allama Iqbal Open University, Islamabad 44000, Pakistan*
[4]*Department of Physics, Hakim Sabzevari University, Sabzevar 96814, Iran*

Correspondence should be addressed to Imad Khan; imadkhan723@gmail.com

Received 15 November 2015; Accepted 28 January 2016

Academic Editor: Maria N. D. S. Cordeiro

We communicate theoretical results of the structural, electronic, and optical properties of ZnO_xTe_{1-x} ($0 \le x \le 1$) in the zincblende structure. The calculations are performed using full potential linearized augmented plane waves (FP-LAPW) method, based on density functional theory (DFT). The structural properties are calculated with simple GGA (PBEsol), while the electronic and optical properties are calculated using mBJ-GGA. The mBJ-GGA is used to properly treat the active d-orbital in their valence shell. The ZnOTe alloy is highly lattice mismatched and consequently the lattice constants and bulk moduli largely deviate from the linear behavior. The calculated bandgaps are in agreement with the experimentally measured values, where the nature of bandgaps is direct for the whole range of x except at $x = 0.25$. We also calculate the bandgap bowing parameter from our accurate bandgaps and resolve the existing controversy in this parameter.

1. Introduction

Solar radiations are widely spread, environment-friendly, and permanent natural source of energy. Different techniques such as photochemical, photothermal, and photoelectrical conversions are being used to convert sunlight into other forms of energies [1]. The concept of intermediate band solar cell (IBSC) materials has attracted great attention for efficient solar energy convergence [2–6]. Both quantum dots and highly mismatched alloys (HMAs) are renowned for IBSC [3, 4, 7]. HMAs are mostly referred to as dilute III-V nitride and II-VI oxide semiconductors. Because of the huge difference in the size and electronegativity between nitrogen/oxygen atom and other group V/VI atoms in the III-V/II-VI host materials, such as N in GaAs or O in ZnTe, deep level states may be formed when nitrogen/oxygen atoms are replaced by the group V/VI atoms. Besides IBSC, these HMAs are of special interest because their bandgaps and other physical properties change greatly with anion/cation compositions [8]. These materials are important from bandgap engineering point of view and their bandgaps can be tuned for their effective use in optoelectronic devices and solar cells.

Wide bandgap semiconductors ZnO, ZnTe, and their ternaries and quaternaries II-VI alloys are known as functional materials in solid state devices including light detectors and emitters operating in the visible and ultraviolet range of electromagnetic spectrum and transparent electronics [9]. The IBSC in ZnOTe is predicted using Band Anticrossing (BAC) model [10], with a theoretical efficiency of 63%, demonstrated by Lee and Wang [11]. Due to the wide range of applications, the alloy has been extensively studied experimentally using different techniques [3, 5, 12–18]. All of these experimental reports concluded that ZnOTe in the zincblende crystal structure is a precious material for optoelectronic devices. They observed reduction in the bandgap with the increase in oxygen concentration. Similar behavior

(reduction in the bandgap) is also observed in the experimental studies of ZnOSe [19]. This reduction is evident from the bowing behavior of the bandgaps as a function of the composition x. The deviation from linear behavior is often described by bowing parameter b. The subject for ZnOTe is experimentally investigated by Merita et al. [16] and theoretically by Moon et al. [20], where both studies suggest further investigation of the bowing parameter. Bouarissa et al. [21] investigated the elastic and vibrational properties of the compound using density functional perturbation theory, while the dielectric and optical properties have been reported by Zerroug et al. [22] and Gueddim et al. [23] using Engel and Vosko exchange correlation functional (EV-GGA).

In the present study the structural, electronic, and optical properties as well as bandgap bowing parameter of ZnTeO are investigated theoretically, to examine the effect on the physical properties of the crystal with the increase in oxygen concentration. The strong p-d coupling between Zn-d and group VI-p states makes these alloys strongly correlated electron systems, and this strong p-d coupling cannot be treated with the ordinary DFT exchange and correlation approximations like LDA and GGA. Modified Becke and Johnson (mBJ) exchange potential is very efficient in solving such problems up to great extent; therefore, in the present theoretical studies, mBJ potential is used within the FP-LAPW method to investigate the optical bandgaps and other physical properties of ZnOTe.

2. Computational Details

The physical properties of a material are sensitive to its structural geometry and correlation of nearby neighboring atoms and molecules [24]. The effects of local correlation of the atomic arrangements on the stability of a crystal are important; therefore the supercells are modeled using SQS method developed by Zunger et al. [24], in which short and intermediate range correlations are considered. In the present work $1 \times 1 \times 1$ supercell having 8 atoms is used.

The calculations are performed using the FP-LAPW method within the framework of the DFT as implemented in the Wien2k package [25]. The exchange and correlation potentials of the generalized gradient approximation (GGA-PBE-sol) are used for the calculation of the structural properties, while for the electronic and optical properties in addition to GGA we also used modified Becke-Johnson (mBJ) exchange potential [26]. The mBJ approach is very successful in the prediction of the bandgaps of the II-VI semiconductors [27–33]. In the FP-LAPW method the potential and charge density are expanded in spherical harmonics inside the nonoverlapping spheres (muffin-tin spheres) and in plane waves basis set in the remaining space of the unit cell (interstitial region). For the wave function expansion inside the atomic spheres, the value of l is confined to $l_{\max} = 10$ and for interstitial nonspherical part $l_{\max} = 6$. The muffin-tin radii are used in such a way that no charge leakage from the core takes place and the total energy is converged. For the wave function in the interstitial region the plane wave cutoff value of $K_{\max}$ is $7/R_{\mathrm{MT}}$, while the charge density is Fourier expanded up to $G_{\max} = 12$ (Ry). The Brillouin zone integration is performed using a mesh of 2000 k points, and convergence is checked through self-consistency.

3. Results and Discussions

3.1. Structural Properties. The favorable state for ZnOTe is cubic zincblende structure at ambient pressure. Therefore, the alloys are modeled in steps of 0.25 in this structure and each unit cell is optimized by minimizing the total energy with respect to the cell volume, as done in our previous work [39]. The lattice constants and bulk moduli are evaluated by fitting the total energy versus unit cell volume to Murnaghan's equation of state [40]. The calculated lattice constants and bulk moduli of ZnO_xTe_{1-x} at different concentrations of O are summarized in Table 1.

Our calculated lattice constant for ZnTe (6.09 Å) is in agreement with the experimental value (6.10 Å) [34], whereas the lattice constant of ZnO (4.58 Å) is slightly overestimated compared to the experimentally (4.47 Å) reported result [35]. This overestimation can be related to the fact that GGA generally overestimates lattice constants and underestimates bandgaps due to the lack of electrons correlation effects. In comparison with the results of [29, 37], our results of binary semiconductors are much closer to the experimental ones [34, 35]. This can be related to the use of different GGA schemes (PBEsol) in the calculations. The variation in the lattice constant and bulk modulus of the ZnO_xTe_{1-x} with the increasing oxygen concentration is shown in Figure 1(a). From the figure it is obvious that the lattice constant is decreasing with the increase in oxygen concentration. This decrease in the lattice constant is related to the smaller size of oxygen than tellurium.

Generally, in ordered alloys it has been observed that the physical properties of the alloy vary linearly with the compositions x, whereas this linear behavior can be explained by Vegard's law [41]. From Figure 1(a) it is obvious that lattice constant does not obey Vegard's law and deviates largely from linear behavior. This deviation is due to the fact that the alloy is highly lattice mismatched and hence there is a large difference in the lattice constants of ZnTe (6.09 Å) and ZnO (4.58 Å). It is also clear from Figure 1 that both the present and reported results [22] of the lattice constants are larger than those of linear fit. The bulk modulus is a very meaningful mechanical parameter of the compound and is also plotted against concentration x in Figure 1(b). Our calculated result for the bulk modulus of ZnTe (45.94 GPa) is in agreement with the experimentally measured value (52.8 GPa) [34], whereas the other reported theoretical results [21, 29] are slightly overestimated compared to the experimental value. In ZnO our calculated result (168 GPa) is in agreement with the reported value of 168 GPa [36]. Bouarissa et al. [21] reported the bulk modulus for ZnO using elastic stiffness coefficients and their evaluated value is too much overestimated as compared to presently calculated data and also reported in [36]. From Figure 1(b) it can be seen that the bulk modulus increases with the increase in O composition. The increase in the bulk modulus is nonlinear and deviates largely from Vegard's law. This deviation is also found by Zerroug et al. [22] but the results are underestimated with respect to present

Table 1: Calculated lattice constants, bulk moduli, and bandgaps compared with experimental and other theoretical results.

X	Lattice constant (Å)			Bulk modulus, B (GPa)			Bandgap (eV)		
	Exp.	Theoretical		Exp.	Theoretical		Exp.	Theoretical	
		Present	Other		Present	Other		Present	Other
0	6.10[a]	6.09	6.011[b]	52.8[a]	45.94	55.36[i], 55.44[b]	2.39[a]	2.39	2.39[f]
1/4		5.96			49.80			1.70	
1/2		5.53			88.85	153.68[i]		1.40	
3/4		5.12			120.94			2.38	
1	4.47[c]	4.58	4.60[e]		168.39	168[d], 252[i]	3.19[g]	3.15	3.15[h]

[a]Ref. [34]. [b]Ref. [29]. [c]Ref. [35]. [d]Ref. [36]. [e]Ref. [37]. [f]Ref. [33]. [g]Ref. [38]. [h]Ref. [31]. [i]Ref. [21].

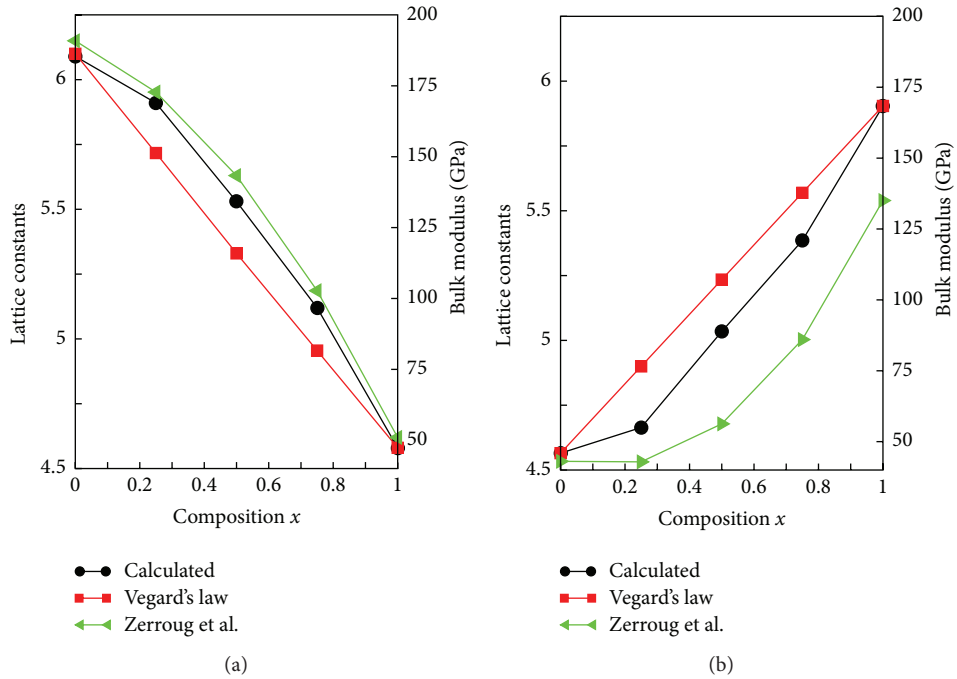

Figure 1: Variation of (a) lattice constant and (b) bulk modulus of ZnOTe with concentration x.

results. These deviations in lattice constants and bulk moduli are due to the large mismatch in the electronegativity between the constituting atoms Zn (1.65), Te (2.1), and O (3.44) and the structure deformation; this is a common trend in II^B-VI ternary semiconductors [31].

3.2. Electronic Properties. Band structure is a key parameter in solid state semiconductors, because almost all physical properties of materials are directly or indirectly related to the energy gap. Both binary ZnTe and ZnO are wide and direct bandgap semiconductors and the calculated bandgap energies of these materials are listed in Table 1. From the table it is clear that our calculated results for the binaries are in agreement with the experimental [34, 38] and other theoretical results [31, 33], which confirms the validation of our theoretical model (mBJ). The calculated bandgaps of ZnO_xTe_{1-x} (x = 0.25, 0.50, 0.75) are shown in Figures 2(a)–2(c), and the corresponding numerical values are presented in Table 1. From the figure it is clear that at 25% of O concentration the alloy has an indirect bandgap of 1.7 eV at Γ-R and direct bandgap of 1.8 eV at Γ-Γ symmetry points of the Brillouin zone. With the substitution of oxygen in ZnTe, the energy states are rearranged and the direct nature of the bandgap shifts to indirect. The conversion of direct to indirect bandgap in ZnOTe can be related to the large difference in the sizes and the electronegativities of Te and O. Gueddim et al. [23] studied ZnO_xTe_{1-x} with oxygen concentration up to 6.25% and confirmed the direct band nature of the material.

The material has direct bandgaps at 50% and 75% of oxygen concentration. From the table it is clear that the bandgap decreases up to 1.4 eV at x = 0.50 and then it increases. The reduction in the calculated bandgap is in agreement with the experimental results [16, 17]. The variation in the bandgap with concentration x is shown in Figure 3, which is also compared with the theoretical results of Moon et al. [20]. The figure shows that the bandgap energy deviates largely from the linear behavior and therefore large bowing is expected. This deviation and this conversion

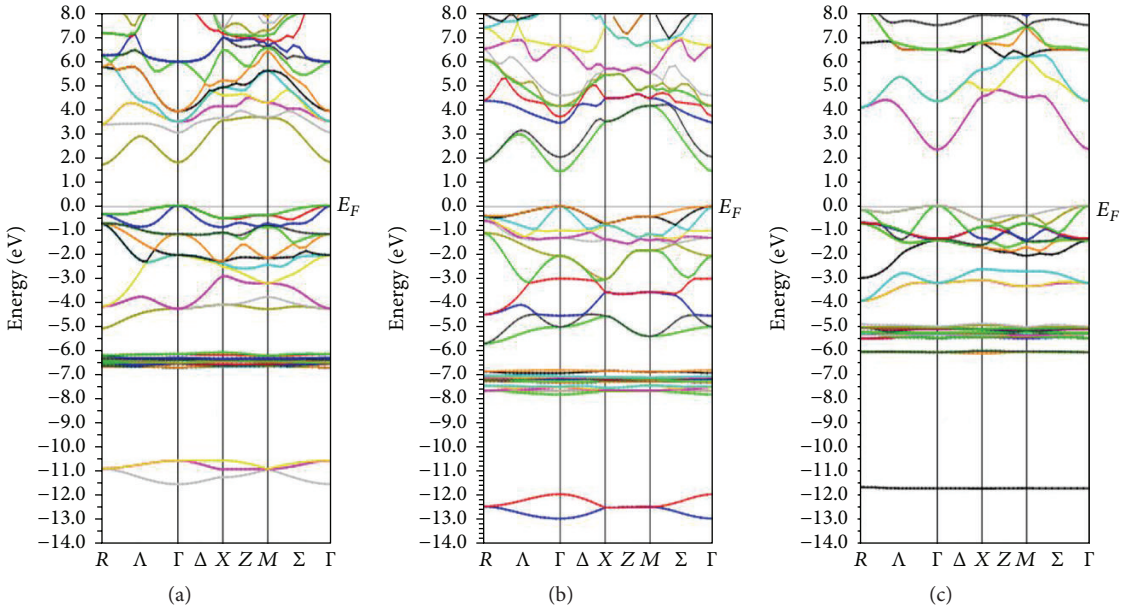

FIGURE 2: Bandgap energies of (a) $ZnO_{0.25}Te_{0.75}$, (b) $ZnO_{0.50}Te_{0.50}$, and (c) $ZnO_{0.75}Te_{0.25}$.

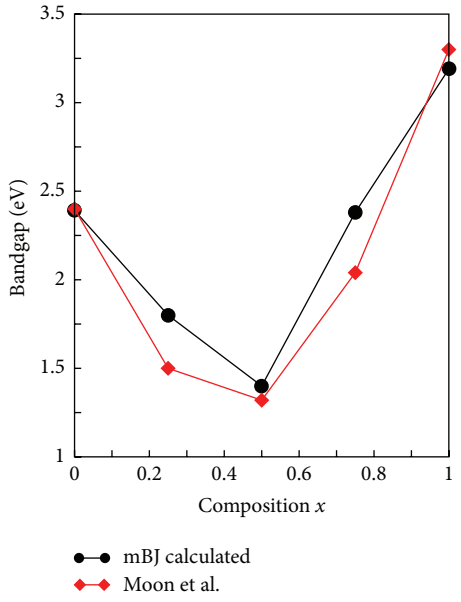

FIGURE 3: Bandgap energy as function of composition x.

from direct to indirect bandgap are because of the large electronegativity difference between Te and O, variation of bond nature, volume deformation, and charge transfer [42]. The bowing parameter b is composition dependent and it is nearly constant near $x = 0.5$ but increases significantly at the dilute limits. From the plot it is clear that the bandgap is decreased significantly by adding only small percent of O into ZnTe or Te into ZnO. This is due to the large size and chemical mismatch between Te and O. Adding more electronegative O to ZnTe creates an isovalent defect level below the conduction band minimum (CBM), whereas adding the less electronegative Te to ZnO creates a deep isovalent defect level above the valence-band maximum (VBM) in the impurity limit. Because of this, the wave function of the band-edge states in the dilute limit is strongly localized, and the bowing coefficient is therefore large, resulting in the decrease in the bandgap. At $x = 0.5$, the defect levels hybridize with the host states and couple between themselves, forming defect bands. In this band like region, the band-edge wave functions become more delocalized than in the dilute limit, so the bowing coefficients become smaller and nearly constant [20], and the dip in the bandgap is observed at $x = 0.50$.

From Figure 3 it is clear that the bandgaps calculated by Moon et al. [20] are underestimated; this discrepancy is associated with the model used (GGA) which underestimates bandgaps. Though the bandgap bowing parameter is previously calculated both experimentally [16] and theoretically [20], both have ambiguous results and suggested further investigations of the bowing parameter. In the present theoretical work we calculate the bowing parameter by using (1) and quadratic fit equation, that is, (2) as given below [31]:

$$E_g\left(ZnO_xTe_{1-x}\right) = E_g\left(ZnO\right)(x) + E_g\left(ZnTe\right)(1-x) - b\,(x)\,(1-x)\,, \tag{1}$$

$$E_g\left(ZnO_xTe_{1-x}\right) \Longrightarrow 2.37 - 3.99x + 4.91x^2. \tag{2}$$

The average bowing parameter calculated by using (1) is 4.83 eV and by (2) is 4.91 eV, which are close to each other. It is expected that the experimental bowing parameter will be around 4.9 eV, because we expect that our calculated bandgaps will be in closer agreement with the experimental values.

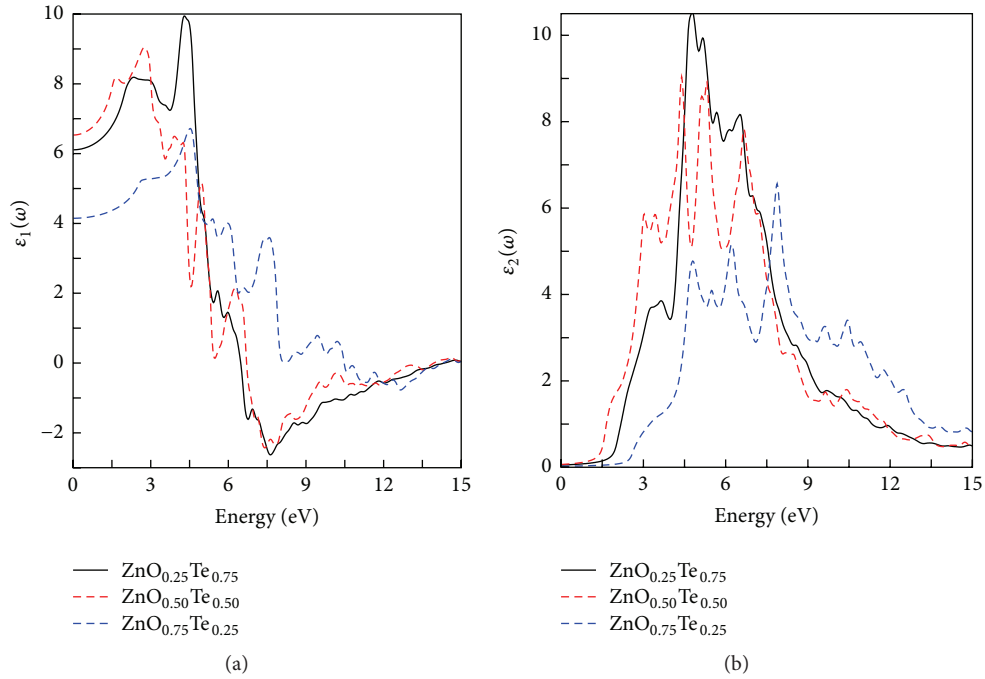

Figure 4: Frequency dependent (a) real and (b) imaginary part of dielectric function.

3.3. Optical Properties. The wide range of bandgap energies (2.39–3.15 eV) of ZnO_xTe_{1-x} makes this material attractive for optoelectronic devices. Therefore it is necessary to attain accurate knowledge of the optical properties like dielectric functions, refractive index, reflectivity, and energy loss function of these compounds. The topic was recently reported in [22, 23] using EV-GGA exchange and correlation functional which needs to be dealt with using a better theoretical model to obtain more accurate results. In the present study we revisit the dielectric functions of the compound with the most accurate theoretical model mBJ-GGA. In this study other optical parameters such as refractive index, reflectivity, energy loss function, and oscillator strength are also investigated.

The real part of the complex dielectric function has been displayed in Figure 4(a). The values of the static dielectric function $\varepsilon_1(0)$ are 6.1, 6.5, and 4.1, for $ZnO_{0.25}Te_{0.75}$, $ZnO_{0.50}Te_{0.50}$, and $ZnO_{0.75}Te_{0.25}$ having direct bandgap energies 1.8, 1.4, and 2.38 eV, respectively. This shows that larger bandgap materials yield smaller dielectric constants and smaller bandgap materials yield larger dielectric constants. From the static dielectric function, the real part goes on increasing up to a hump for all concentrations which can be related to the fundamental bandgaps of compounds. The real part of dielectric function $\varepsilon_1(\omega)$ reaches its maximum value for $ZnO_{0.25}Te_{0.75}$, $ZnO_{0.5}Te_{0.5}$, and $ZnO_{0.75}Te_{0.25}$ corresponding to the incident photon energies 4.4, 2.8, and 4.5 eV.

The imaginary part of complex dielectric function is one of the most important optical parameters because it reflects optical gap as well as optical absorption. Figure 4(b) shows the imaginary part of dielectric function $\varepsilon_2(\omega)$ of ZnO_xTe_{1-x} in the energy range 0–15.0 eV. The offset points are observed at 1.8, 1.5, and 2.4 eV for $ZnO_{0.25}Te_{0.75}$, $ZnO_{0.5}Te_{0.5}$, and $ZnO_{0.75}Te_{0.25}$, respectively. These offset points are related to the fundamental direct bandgaps of these materials. Beyond these points the curves increase abruptly and reach the peak values at energies 5.6 eV for $ZnO_{0.25}Te_{0.75}$ and $ZnO_{0.5}Te_{0.5}$ and 8.0 eV for $ZnO_{0.75}Te_{0.25}$.

Refractive index explains the ability of a material to permit or bend light as it passes through it. The normal refractive index versus energy plot has been displayed in Figure 5(a). At zero frequency limit $n(0)$, its values are 2.45, 2.55, and 2.05 for $x = 0.25$, 0.50, and 0.75, respectively. From these calculated values it is clear that a larger bandgap material yields smaller value of refractive index and vice versa, as observed in the real part of dielectric functions. With the increasing incident photon energy, the normal refractive indices increase up to humps which correspond to the fundamental bandgaps. The refractive indices reach peak values of 3.33, 3.06, and 2.66 for different concentrations. Beyond these peak values the refractive indices decrease abruptly with some variations and drop below unity at energies 8 eV for $ZnO_{0.25}Te_{0.75}$ and $ZnO_{0.50}Te_{0.50}$ and 11 eV for $ZnO_{0.75}Te_{0.25}$. This is because refractive index measures phase velocity, which does not carry any information. Phase velocity is the speed at which the crests of a wave move and can be faster than the speed of light and thereby gives a refractive index below unity.

The influence of oxygen concentration in ZnTe can be precisely measured from reflectivity spectra. The reflectivity $R(\omega)$ is plotted against the incident photon frequency in Figure 5(b). The peaks in the figure show that each concentration has a maximum value of reflectivity. The maximum lies in the energy range 7–12 eV and arises from the interband transitions. The plot also clarifies that with the increase in the oxygen concentration the reflectivity is decreased, which

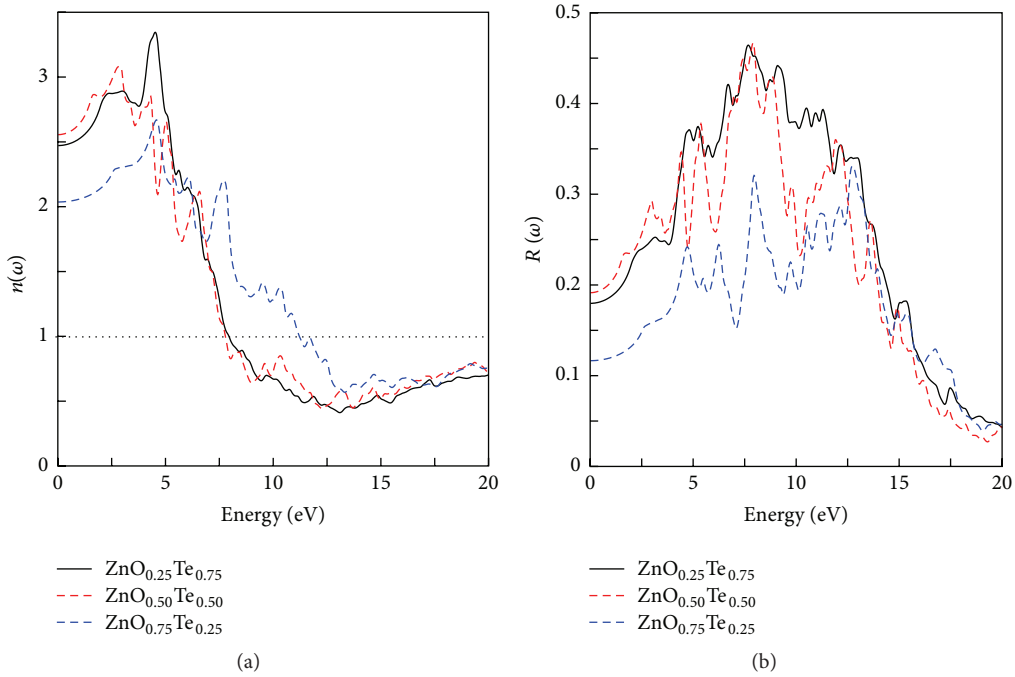

FIGURE 5: Frequency dependent (a) refractive index and (b) reflectivity.

means that the insulating behavior of the compound becomes more dominant.

The energy loss function is an important parameter, which describes the energy loss of an incident photon while traversing through a material medium. During the propagation some of the electrons undergo inelastic scattering and their paths are slightly and randomly deflected. Inelastic interactions include phonon excitations, inter- and intraband transitions, plasmon excitation, and inner shell ionization. The energy loss in inelastic scattering can be theoretically measured via electron energy loss function. The electron energy loss function for ZnOTe ($0.25 \leq x \leq 0.75$) is plotted in Figure 6(a). From the figure it is obvious that if the incident photon energy is lower than the bandgap, then no energy loss occurs, meaning electrons are not responding to the incident photons. In the intermediate energy range, significant energy losses are observed and reach maximum values in the energy range 15–17 eV. These peaks in the energy loss spectra represent the characteristic associated with the plasma resonance and the corresponding frequency is called plasma frequency, above which the material exhibits metallic behavior whereas below which the material has a dielectric property. The peaks shift towards higher energy ranges with the increase in bandgap.

To investigate the number of valence electrons involved in the interband transition per unit cell, we evaluate the oscillator strength sum rule. Oscillator strength is a dimensionless quantity that expresses the probability of absorption or emission of electromagnetic radiation in transitions between energy levels of an atom or molecule. The effective number of electrons which contribute to transition from valence band to conduction band is dependent upon the frequency of the incident light photons [21, 42]. The oscillator strength sum rule for ZnO_xTe_{1-x} is displayed in Figure 6(b). The effective number of electrons which transfer from valence band to conduction band is zero for energy less than 2.5 eV. Beyond this critical energy, a rapid increase is observed in the effective number of electrons. Saturation in the electron number occurs beyond 30 eV. It is also evident from the plot that the effective number of electrons decreases with the increase in the oxygen concentration. This is due to the fact that the atomic number of oxygen is very small as compared to tellurium atom.

4. Conclusions

The structural, electronic, and optical properties of ZnO_xTe_{1-x} ($0 \leq x \leq 1$) are calculated in the zincblende structure using the FP-LAPW method. It is concluded that the calculated lattice constant and bulk modulus of ZnO_xTe_{1-x} deviate largely from the linear behavior with x and do not obey Vegard's law. It is also found that the mBJ-GGA exchange and correlation potentials are very efficient in reproducing the experimental bandgaps of ZnOTe, which concludes direct bandgap nature for the whole range of concentration except $x = 0.25$. Furthermore, reduction in the bandgap with the increase in x has been observed and a dip is found at $x = 0.50$, which is consistent with the experiments. The previously controversial bandgap bowing parameter is revisited with a more realistic approach and a reasonably accurate result is obtained for the bowing parameter. As the material is precious for optoelectronic devices, optical properties like

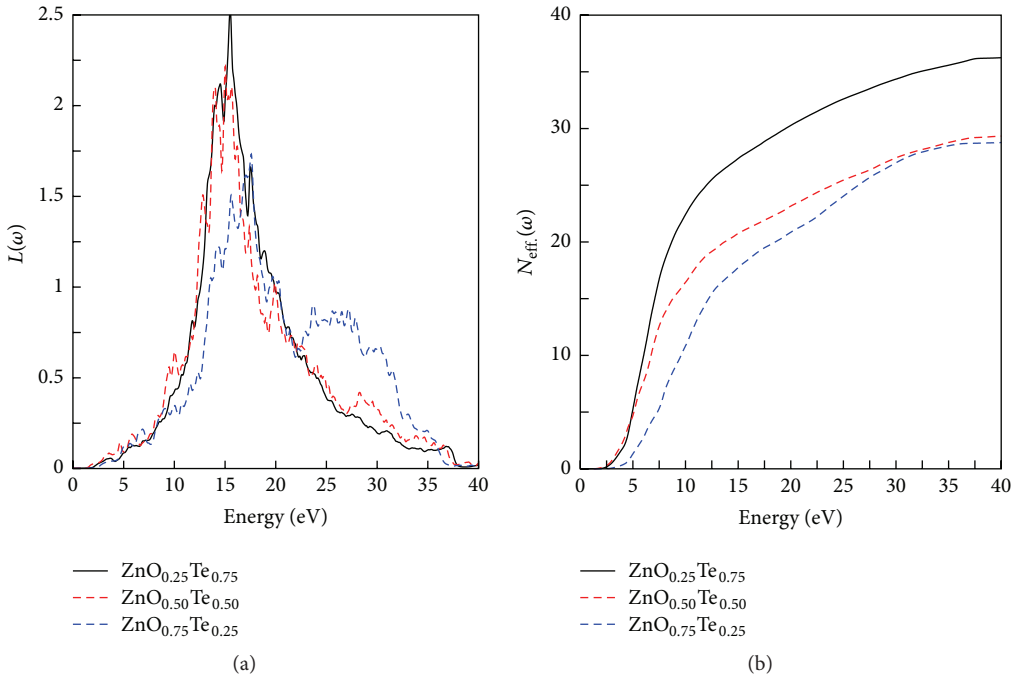

Figure 6: Frequency dependent (a) energy loss function and (b) oscillator strength.

dielectric functions, refractive index, reflectivity, energy loss function, and sum rules are also presented and discussed in detail.

Conflict of Interests

The authors declare that there is no conflict of interests regarding the publication of this paper.

References

[1] R. Iqbal, I. Khan, H. A. R. Aliabad, Z. Ali, and I. Ahmad, "Density functional studies of magneto-optic properties of CdCoS," *Journal of Magnetism and Magnetic Materials*, vol. 351, pp. 60–64, 2014.

[2] A. Luque and A. Martí, "Increasing the efficiency of ideal solar cells by photon induced transitions at intermediate levels," *Physical Review Letters*, vol. 78, no. 26, pp. 5014–5017, 1997.

[3] K. M. Yu, W. Walukiewicz, J. Wu et al., "Diluted II-VI oxide semiconductors with multiple band gaps," *Physical Review Letters*, vol. 91, no. 24, Article ID 246403, 2003.

[4] K. M. Yu, W. Walukiewicz, J. Wu et al., "Diluted ZnMnTe oxide: a multi-band semiconductor for high efficiency solar cells," *Physica Status Solidi (B)*, vol. 241, no. 3, pp. 660–663, 2004.

[5] W. Wang, A. S. Lin, and J. D. Phillips, "Intermediate-band photovoltaic solar cell based on ZnTe:O," *Applied Physics Letters*, vol. 95, no. 1, Article ID 011103, 2009.

[6] Y. Seminovski, P. Palacios, and P. Wahnon, "Obtaining an intermediate band photovoltaic material through the Bi insertion in CdTe," *Solar Energy Materials & Solar Cells*, vol. 114, pp. 99–103, 2013.

[7] N. Lopez, L. A. Reichertz, K. M. Yu, K. Campman, and W. Walukiewicz, "Engineering the electronic band structure for multiband solar cells," *Physical Review Letters*, vol. 106, Article ID 028701, 2011.

[8] C.-Y. Chen, C.-Y. Yang, J.-I. Chyi, and C.-H. Wu, "Optical and electrical properties of ZnSeO alloys grown by plasma-assisted molecular beam epitaxy," *Journal of Crystal Growth*, vol. 378, pp. 180–183, 2013.

[9] J. D. Cuthbert, J. J. Hopfield, and D. G. Thomas, "Znte:o electroluminescent device," USA Patent, 3413506, 1966.

[10] J. Wu, W. Shan, and W. Walukiewicz, "Band anticrossing in highly mismatched III-V semiconductor alloys," *Semiconductor Science and Technology*, vol. 17, no. 8, pp. 860–869, 2002.

[11] B. Lee and L. Wang, "Electronic structure of ZnTe:O and its usability for intermediate band solar cell," *Applied Physics Letters*, vol. 96, no. 7, Article ID 071903, 2010.

[12] Y. Nabetani, T. Okuno, K. Aoki, T. Kato, T. Matsumoto, and T. Hirai, "Epitaxial growth and optical investigations of ZnTeO alloys," *Physica Status Solidi (A)*, vol. 203, no. 11, pp. 2653–2657, 2006.

[13] R. A. Faulkner, "Toward a theory of isoelectronic impurities in semiconductors," *Physical Review*, vol. 175, no. 3, pp. 991–1009, 1968.

[14] J. L. Merz, "Isoelectronic oxygen trap in ZnTe," *Physical Review*, vol. 176, no. 3, article 961, 1968.

[15] M. J. Seong, I. Miotkowski, and A. K. Ramdas, "Oxygen isoelectronic impurities in ZnTe: photoluminescence and absorption spectroscopy," *Physical Review B*, vol. 58, no. 12, pp. 7734–7739, 1998.

[16] S. Merita, T. Krämer, B. Mogwitz, B. Franz, A. Polity, and B. K. Meyer, "Oxygen in sputter-deposited ZnTe thin films," *Physica Status Solidi C*, vol. 3, no. 4, pp. 960–963, 2006.

[17] T. Tanaka, K. M. Yu, A. X. Levander et al., "Demonstration of $ZnTe_{1-x}O_x$ intermediate band solar cell," *Japanese Journal of Applied Physics*, vol. 50, no. 8, Article ID 082304, 2011.

[18] Y. Nabetani, T. Okuno, K. Aoki, T. Kato, T. Matsumoto, and T. Hira, "Photoluminescence properties of ZnTeO and ZnSeO alloys with dilute O concentrations," *Physica Status Solidi (C)*, vol. 3, no. 4, pp. 1078–1081, 2006.

[19] Y. Nabetani, T. Mukawa, Y. Ito, T. Kato, and T. Matsumoto, "Epitaxial growth and large band-gap bowing of ZnSeO alloy," *Applied Physics Letters*, vol. 83, no. 6, pp. 1148–1150, 2003.

[20] C.-Y. Moon, S.-H. Wei, Y. Z. Zhu, and G. D. Chen, "Band-gap bowing coefficients in large size-mismatched II–VI alloys: first-principles calculations," *Physical Review B*, vol. 74, no. 23, Article ID 233202, 2006.

[21] N. Bouarissa, S. A. Siddiqui, A. Hajry, S. Saib, and M. Boucenna, "Elastic properties and lattice vibration modes in $ZnTe_{1-x}O_x$," *Computational Materials Science*, vol. 83, pp. 22–26, 2014.

[22] S. Zerroug, A. Gueddim, M. A. Khan, and N. Bouarissa, "Ab initio study of structural parameters and optical properties of $ZnTe_{1-x}O_x$," *Superlattices and Microstructures*, vol. 53, pp. 155–162, 2013.

[23] A. Gueddim, S. Zerroug, and N. Bouarissa, "Optical characteristics of $ZnTe_{1-x}O_x$ alloys from first-principles calculations," *Journal of Luminescence*, vol. 135, pp. 243–247, 2013.

[24] A. Zunger, S.-H. Wei, L. G. Ferreira, and J. E. Bernard, "Special quasirandom structures," *Physical Review Letters*, vol. 65, no. 3, pp. 353–356, 1990.

[25] P. Blaha, K. Schwarz, G. K. H. Madsen, D. Kvasnicka, and J. Luitz, *WIEN2k: An Augmented Plane Wave Plus Local Orbitals Program for Calculating Crystal Properties*, Vienna University of Technology, Vienna, Austria, 2001.

[26] F. Tran and P. Blaha, "Accurate band gaps of semiconductors and insulators with a semilocal exchange-correlation potential," *Physical Review Letters*, vol. 102, Article ID 226401, 2009.

[27] I. Khan, I. Ahmad, H. A. Rahnamaye Aliabad, and M. Maqbool, "Effect of phase transition on the optoelectronic properties of $Zn_{1-x}Mg_xS$," *Journal of Applied Physics*, vol. 112, no. 7, Article ID 073104, 2012.

[28] I. Khan, F. Subhan, I. Ahmad, and Z. Ali, "Structural and opto-electronic properties of Mg substituted ZTe (Z=Zn, Cd and Hg)," *Journal of Physics and Chemistry of Solids*, vol. 83, pp. 75–84, 2015.

[29] H. H. Gürel, Ö. Akinci, and H. Ünlü, "First principles calculations of Cd and Zn chalcogenides with modified Becke-Johnson density potential," *Superlattices and Microstructures*, vol. 51, no. 5, pp. 725–732, 2012.

[30] I. Khan, I. Ahmad, H. A. R. Aliabad, S. J. Asadabadi, Z. Ali, and M. Maqbool, "Conversion of optically isotropic to anisotropic CdS_xSe_{1-x} $(0 \leq x \leq 1)$ alloy with S concentration," *Computational Materials Science*, vol. 77, pp. 145–152, 2013.

[31] I. Khan and I. Ahmad, "Theoretical studies of the band structure and optoelectronic properties of ZnO_xS_{1-x}," *International Journal of Quantum Chemistry*, vol. 113, no. 9, pp. 1285–1292, 2013.

[32] I. Khan, I. Ahmad, D. Zhang, H. A. Rahnamaye Aliabad, and S. Jalali Asadabadi, "Electronic and optical properties of mixed Be-chalcogenides," *Journal of Physics and Chemistry of Solids*, vol. 74, no. 2, pp. 181–188, 2013.

[33] I. Khan, H. A. R. Aliabad, W. Ahmad, Z. Ali, and I. Ahmad, "First principle optoelectronic studies of visible light sensitive CZT," *Superlattices and Microstructures*, vol. 63, pp. 91–99, 2013.

[34] O. Madelung, Ed., *Landolt Bornstein: Numerical Data and Functional Relationships in Science and Technology*, vol. 17b, Springer, Berlin, Germany, 1982.

[35] A. B. M. A. Ashrafi, A. Ueta, A. Avramescu et al., "Growth and characterization of hypothetical zinc-blende ZnO films on GaAs(001) substrates with ZnS buffer layers," *Applied Physics Letters*, vol. 76, no. 5, pp. 550–552, 2000.

[36] B. Amrani, I. Chiboub, S. Hiadsi, T. Benmessabih, and N. Hamdadou, "Structural and electronic properties of ZnO under high pressures," *Solid State Communications*, vol. 137, no. 7, pp. 395–399, 2006.

[37] Ü. Özgür, Y. I. Alivov, C. Liu et al., "A comprehensive review of ZnO materials and devices," *Journal of Applied Physics*, vol. 98, no. 4, Article ID 041301, 2005.

[38] S. Locmelis, C. Brünig, M. Binnewies et al., "Optical band gap in the system $ZnO_{1-x}S_x$. An experimental and quantum chemical study," *Journal of Materials Science*, vol. 42, no. 6, pp. 1965–1971, 2007.

[39] I. Khan, I. Ahmad, B. Amin, G. Murtaza, and Z. Ali, "Bandgap engineering of $Cd_{1-x}Sr_xO$," *Physica B: Condensed Matter*, vol. 406, no. 13, pp. 2509–2514, 2011.

[40] F. D. Murnaghan, "The compressibility of media under extreme pressures," *Proceedings of the National Academy of Sciences of the United States of America*, vol. 30, pp. 244–247, 1944.

[41] L. Vegard, "Formation of mixed crystals by solid-phase contact," *Journal of Physics*, vol. 5, no. 5, pp. 393–395, 1921.

[42] F. Wooten, *Optical Properties of Solids*, Academic Press, New York, NY, USA, 1972.